NANO LETTERS

2007
Vol. 7, No. 8
2281−2290

# Core-like Particles of an Enveloped Animal Virus Can Self-Assemble Efficiently on Artificial Templates

**Nancy L. Goicochea,[†] Mrinmoy De,[§] Vincent M. Rotello,[§] Suchetana Mukhopadhyay,*[,‡] and Bogdan Dragnea*[,†]**

*Department of Chemistry and Department of Biology, Indiana University, Bloomington, Indiana 47405, and Department of Chemistry, University of Massachusetts—Amherst, Amherst, Massachusetts 01002*

*Received April 12, 2007; Revised Manuscript Received June 20, 2007*

## ABSTRACT

**Alphaviruses are animal viruses holding great promise for biomedical applications as drug delivery vectors, functional imaging probes, and nanoparticle delivery vesicles because of their efficient in vitro self-assembly properties. However, due to their complex structure, with a protein capsid encapsulating the genome and an outer membrane composed of lipids and glycoproteins, the in-vitro self-assembly of virus-like particles, which have the functional virus coat but carry an artificial cargo, can be challenging. Fabrication of such alphavirus-like particles is likely to require a two-step process: first, the assembly of a capsid structure around an artificial core, second the addition of the membrane layer. Here we report progress made on the first step: the efficient self-assembly of the alphavirus capsid around a functionalized nanoparticle core.**

**Introduction.** Commonly associated with pathogenic agents, viruses have recently been revisited with increased interest for their therapeutic potential as drug delivery vectors,[1−3] functional imaging probes,[4,5] and for novel biomaterials or biologically assisted nanomaterial synthesis.[6−9] Three different viral platforms, engineered plant viruses,[10−12] animal viruses,[2,13] and bacteriophages,[14,15] are currently under development for these applications.

Plant viruses and bacteriophages have been proposed as platform technologies for diagnostic imaging because of their low toxicity even at high doses.[8] It has been shown that icosahedral plant virus capsids can encapsulate a spherical nanoparticle with a volume of up to 2500 $nm^3$ while keeping a close morphological resemblance to the native virus.[16] The artificial cargo, or encapsulated material, did not need to be prepared inside a pre-existing virus capsid, thus there were no compatibility constraints to the cargo synthesis environment. Rather, capsid and cargo were self-assembled in conditions similar to those used in the in vitro preparation of infectious viruses from isolated components.[4,17−19] Nevertheless, plant viruses and bacteriophages have their limitations. Even though residues can be engineered at the virus surface, allowing recognition by cell surface receptors of a particular type of cell, such as cancer cells,[20,21] plant viruses are incapable of passing the blood stream and elicit a strong response from the host.[8,21,22] The use of bacteriophages as delivery vectors[14] faces similar challenges.

When specific delivery of therapeutic molecules is sought, animal viruses have efficient built-in mechanisms of cellular entry that are absent in the case of plant or bacteriophage viruses.

While the idea of using any animal viruses possessing a genome in humans represents a risk because of the possibility of spontaneous mutation and replication of the viral particles[2,8,13] the use of nanoparticles instead of a complete genome would alleviate this problem. Thus animal viruses provide an alternative platform for nanoparticle diagnostic or delivery vectors. Animal viruses that can be naturally recognized by cell receptors of specific types of cells[8,23] are of particular interest because this increases the specificity of the nanoparticle itself for uses in biomedical applications or as functional imaging probes. To this end, we have selected alphaviruses as a platform for nanoparticle delivery.

Alphaviruses are small, icosahedral, enveloped viruses that cause disease in humans and domestic animals.[24] The ability to carry out in vitro assembly of corelike alphavirus particles[25−28] has made them a good candidate for bionanotechnological applications.

With respect to the viruses discussed by Singh et al.,[8] the alphavirus infection starts with receptor-mediated endocytosis.[24] In this process, viruses bound to receptors on the cell surface are taken up into endosomes. The low pH present

* Corresponding authors. E-mail: sumukhop@indiana.edu (S.M.); dragnea@indiana.edu (B.D.).
[†] Department of Chemistry, Indiana University.
[‡] Department of Biology, Indiana University.
[§] Department of Chemistry, University of Massachusetts—Amherst.

10.1021/nl070860e CCC: $37.00 
**Published on Web 07/24/2007**

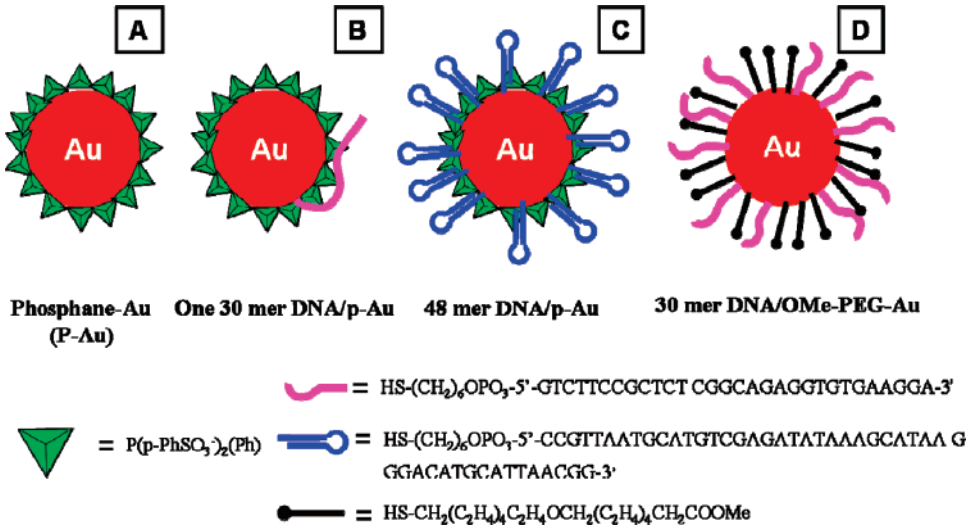


**Figure 1.** Functionalization of Au nanoparticles. (A) phosphane. (B) Phosphane and a single strand of unspecific 30-mer DNA (1 equiv DNA:1 equiv Au). (C) Mixed monolayers of 48-mer DNA and phosphane molecules (2200 equiv DNA:1 equiv Au). (D) Mixed monolayers of 30-mer DNA and OMe-PEG molecules (750 equiv DNA:1 equiv Au).

in the endosomal compartment activates fusion activity in the viral surface proteins. The ensuing fusion between the viral and the endosomal membranes allows the penetration of the viral core into the cytoplasm through a so-called fusion pore.[29] A large number of viruses infect cells by this route (see ref 29 for a review). The endocytotic pathway distinguishes the alphavirus from plant and bacteriophage virus platforms tested for biomedical nanotechnology applicatons.

Cryo-EM imaging and 3D image reconstructions confirmed that alphaviruses contain a lipid bilayer sandwiched between an external glycoprotein membrane and an internal nucleocapsid core.[28,30−34] The two concentric protein shells are interconnected across the lipid membrane with pseudo-$T = 4$ icosahedral symmetry. The nucleocapsid self-assembles from 240 identical protein subunits and measures 39 nm, while the inner cavity encapsulating the genome has a diameter of ~33 nm.[30,31,33] The genomic RNA, 11.7 kb in length, is encapsulated within the nucleocapsid.[35] The cDNA sequence of many of these viruses is known, making them ideal for vector expression models for gene/drug delivery and cancer therapy and neuron chemical synapses.[8,23,36−39] In this context, alphaviruses represent an ideal system because the nucleocapsid core forms independently from the glycoprotein shell in vivo and the nucleocapsid assembly can be reconstituted in vitro. Furthermore, in vivo, alphaviruses can be specifically engineered through site-directed mutagenesis of the glycoprotein E2 to exhibit specific targeting activity toward specific receptors in animal models.[2,13,20,23]

To make an alphavirus-based molecular container, one has to gather insight from the principles of the native virus assembly. Unfortunately, the exact mechanism of in vitro corelike particle (CLP) formation is still unclear and the preparation of infective virus particles in laboratory still requires host cell involvement.[31,40,41] Previous research on CLP assembly has focused on the C-terminal domain of the capsid protein (CP). The N-terminal region is believed to have a random coil organization with the exception of a helical sequence.[27,42,43] As a marked difference from many other in vitro assembly systems,[18,44,45] alphavirus CLPs are believed to form only in presence of single-stranded nucleic acid. Absence of nucleic acid or ds-DNA inhibits CLP assembly.[25] It should be noted, however, that CLPs can also form with tRNA, suggesting the structure of RNA may have more of a role than the sequence.[25,46]

In this work, we exploit in vitro CLP assembly features to form particles that encapsulate a functionalized gold nanoparticle (GNP). Gold nanoparticles have been chosen to test the idea of encapsulation because of their well-known surface chemistry[10,21] and because of their characteristic optical properties.[47]

Two questions are being addressed: The first question is whether nonspecific electrostatic interactions plus the rigidity of a spherical nanoparticle template of different sizes is sufficient to bypass the specific interaction requirement for the in vitro assembly of CLPs. The nanoparticles were functionalized with different ligands, Figure 1: methoxy PEG ligands, negatively charged phosphane molecules, and specific and unspecific sequences of 5′ thiol-modified ss-DNA. Reassembly reactions and product analysis were carried out as a function of core size and ligand.

The second question is whether an increase in stability could be imparted *from the interior* of the nucleocapsid through the incorporation of a solid spherical template. In this context, Forsell et al.[48] have suggested that the outer membrane glycoprotein network has a direct role in stabilizing and organizing the structure of the mature alphavirus particle. In the absence of membrane and glycoproteins, nucleocapsid core particles are fragile, lacking accurate icosahedral symmetry.[28] More stable nucleocapsids should provide a broader range of experimental conditions to choose from upon subsequent attempts of adding lipid membranes and glycoproteins.

The main findings discussed here are: (1) an anionic nanoparticle core is sufficient to promote the association of alphavirus CP with the core, (2) electrostatically driven

core−CP association occurs regardless the size of the nanoparticle template, and (3) among the tested ligands, maximum efficiency of encapsulation has been obtained when GNPs were functionalized with a mixture of phosphane and 48-mer ss-DNA. In this case, the assembly protocol yielded spherical capsids similar in shape and size to the wild type (wt) CLPs. Moreover, the Au-encapsulating CLPs were more stable over time than wt CLPs. Interestingly, we found that the presence of free 48-mer ss-DNA in solution significantly increases the yield of Au−CLP production, which may indicate that nucleoprotein precursors have to form prior to CLP self-organization.

**Materials and Methods.** *I. Synthesis of Functionalized Gold Nanoparticles.* GNPs of different sizes were prepared by citrate reduction of $HAuCl_4$.[49,50] Exchange reactions with different coatings were performed according to established methods described below.

Exchange of Citrate−Au NPs (14 nm) with Carboxylated PEG Ligand (PEG)−COOH. HOOC−PEG−Au NPs were prepared from citrate−Au NPs using a modification of Zhu's method.[18,51] Briefly: PEG-coated GNPs were obtained by adding a large excess of thiol ligand (10 equiv/particle) to citrate−Au NPs solution. The number of equivalents was estimated by assuming that the occupied surface area by a single thiol molecule is 0.2 $nm^2$.[51] The mixture was then stirred at room temperature for 24 h. To eliminate unreacted ligands, the mixture was diluted with 3 volumes of THF and centrifuged at 16 000 rpm (JA 20 rotor) × 30 min at 4 °C. The supernatant was removed and the pellet was redissolved in acidic water (pH ∼ 3) and a second centrifugation was carried out under the same conditions. Finally, the pellet was redissolved in neutral water (pH ∼ 7) and the suspension sonicated for 5 min to ensure complete gold conjugate dispersion in solution.

Exchange of Citrate−Au NPs (10 nm) with Methoxy PEG ligand (PEG)−OMe. Neutral MeO−PEG−Au conjugates were obtained from citrate−Au NPs by ligand exchange reactions according to Zhu's method.[51] Briefly: 10 equiv PEG/particle were added to citrate-stabilized GNPs solution and left stirring for 20 h at room temperature. The mixture was purified by adding 3 volumes of THF and the solution centrifuged at 26 500*g* for 30 min at 4 °C. The supernatant was removed and the pellet redissolved in 10 mL of pure water and 30 mL of THF. A second centrifugation was carried out under the same conditions, and the pellet was redissolved in pure water and sonicated for 5 min to ensure complete gold conjugate solubilization into the solution.

Exchange of MeO−PEG−Au NPs (10 nm) with 30-mer 5′ Thiol-Modified ss-DNA. Generation of a mixed layer containing ss-DNA thiolated at their 5′ end and PEG−OMe on the gold surface was obtained from a small modification of Zhu's protocol.[51] A small amount of surface-attached PEG molecules were exchanged with thiolated ss-DNA using 0.5 DNA equiv/1 PEG equiv (750 DNA equiv/particle).[51] For simplicity, these molecules will be termed as 30-mer DNA/MeO−PEG−Au NPs.

Exchange of Citrate−Au NPs (8.3−27.4 nm) with Bis-(*p*-sulfonatophenyl)phenyl Phosphine Dehydrate. Bis-(*p*-sulfonatophenyl)phenyl phosphine dehydrate ligands (**1**) were exchanged from citrate−Au NPs according to Loweth's protocol.[52] Aqueous solutions (10 mL) of citrate−Au were stirred overnight with a large excess of ligand (20−40 mg) at room temperature. Addition of NaCl induced GNP precipitation followed by separation through centrifugation at 16 000*g* for 40 min and 4 °C. After a second work up, the final pellet was resuspended in a small volume (∼200 $\mu$L) of phosphane solution (25 mg of **1** in 100 mL of water). These particles are termed p−Au nanoparticles.

Exchange of Phosphane−GNPs (10 nm) with a Single Strand of 30-mer 5′ Thiol-Modified ss-DNA. Exchange reactions of phosphane−Au NPs with a single ss-DNA modified with a thiol group at its 5′ end HS-$(CH_2)_6OPO_3$-5′-GTCTTCCGCTCT CGGCAGAGGTGTGAAGGA-3′) were performed according to Zanchet's protocol.[53] Briefly: DNA/phosphane−Au conjugates were prepared by adding 1.1 DNA equiv per particle to phosphane−Au NPs dispersed in 1 mL of 0.5× TBE buffer. To promote the exchange of ligands, the electrostatic repulsion between DNA and phosphane molecules must be lowered by increasing the ionic strength of the reaction mixture (10 $\mu$L of 2.5M NaCl) to reach 50 mM. After shaking for a few seconds, the mixture was allowed to stand for 2 h before concentrating the volume for further use. For simplicity, these particles will be named as one 30-mer DNA/p−Au nanoparticles.

Exchange of Phosphane-GNPs (8.3−27.4 nm) with 48-mer 5′ Thiol-Modified ss-DNA. Generation of a mixed monolayer containing ss-DNA modified with a thiol group at their 5′ end (HS-$(CH_2)_6OPO_3$-5′-CCGTTAATGCATGTC-GAGATATAAAGCATAA GGGACATGCATTAACGG-3′) and phosphane molecules on gold surface was obtained as described in Parak et al.[54] with the following modifications. Prior to DNA exchange, the ionic strength of the phosphane−Au NPs solution was increased to 50−100 mM by adding 1M NaCl. This initial step is crucial to minimize the electrostatic interactions between the phosphate backbone of DNA and the phosphanes on the nanocrystal surface. At the same time, the ionic strength jump promotes reversible GNP flocculation. Thus, the addition of salt is enough to promote thiol attachment while avoiding irreversible aggregation of the nanoparticles. Addition of a large excess of ss-DNA to phosphane−Au nanoparticles (2200 equiv per particle) was used to ensure saturation coverage in ss-DNA. The number of equiv was calculated by assuming that the occupied surface area by a single thiol molecule is ca. 0.20 $nm^2$.[18,51,55,56]

After thiol addition, the reaction mixture was left stirring for 48 h at room temperature, long enough to ensure maximum replacement of oligonucleotides.[54,55] The unreacted ligands were then removed using ultracentrifugation. Subsequent purification was carried out using microcon ultrafilters of 60 kDa nominal molecular weight cutoff (14 000*g* for 45−75 min). The resulting reddish pellet was redissolved in tris-borate-EDTA buffer (TBE 0.5×). For simplicity, these particles will be named 48-mer DNA/p−Au nanoparticles.

*II. Characterization.* Particle (CP or gold particle) concentration and coat composition were obtained by UV−vis

absorption using a Nanodrop ND-1000 UV−vis spectrophotometer. To prevent saturation, 50× diluted aliquots of the master colloidal solutions were used for analysis. The plasmon bands of the differently sized particles (8.3−27.4 nm) were between 520 and 526 nm, as expected.

Dynamic light scattering (DLS, Zetasizer NanoS, Malvern) of functionalized GNPs in TBE buffer was performed to determine the hydrodynamic size increase after functionalization and after Au−CLP assembly. Prior to DLS measurements, all solutions were filtered using a 0.1 $\mu$m syringe filter and sonicated for 30 min to remove large aggregates that would otherwise dominate the scattering, even if in small numbers, due to their large scattering cross section. In the case of DNA/p−Au−CLP, the samples were sonicated in cold water (6 °C) for 30 min and the DLS measurements were taken at 8 °C.

Gel electrophoresis was used to evaluate the purity of the DNA/p−Au conjugates. The matrix was made of 3% agarose gel and EtBr (10 mg/mL) in 1× TBE buffer (0.09 M Tris: 0.09 M Boric acid:2 mM EDTA; pH 8.3). To have a clear visualization of the gold bands, use of concentrated samples (∼100 nM) is required.

Transmission electron microscopy (TEM) data were obtained on a JEOL 1010 equipped with a 4k CCD camera operating at 80 kV. For TEM imaging, the samples were unstained or negatively stained with 1% uranyl acetate. Electron micrographs of gold nanoparticles and Au−CLP were taken by transferring 10 uL of solution to a carbon-coated Formvar copper grid (200 mesh). Solution excess was removed after 20 min and stained (in case of Au−CLP) for another 20 min. The stain excess in the grid was removed with filter paper and the grid was visualized by TEM. Au−CLPs diameters and efficiencies were determined using two or more grids independently prepared, with at least 800 particles imaged per grid.

*III. Efficiency of the Gold Core Size in Promoting 48-mer DNA/p−Au−CLP Assembly.* The encapsidation efficiency was calculated using the following equation:

$$\eta_{\text{total}} = N_{\text{Au-CLP}}/N_{\text{Au}}$$

$N_{\text{Au-CLP}}$ represents the total number of 48-mer DNA/p−Au−CLPs assembled, while $N_{\text{Au}}$ corresponds to the total number of functionalized GNPs at a constant CLP:Au initial ratio of 1:1 equiv. Encapsulation efficiency studies were carried out only with 48-mer DNA/p−Au particles because of their good stability and monodispersity after assembly with CP. It is worth noting here that the way efficiency of encapsulation is defined implies that 100% efficiency would be achieved when all the protein would assemble into Au-filled capsids. The amount of protein that has associated in nonproductive ways (or precipitated) can be estimated from the fraction of Au particles that are not encapsulated in a spherical shell.

A completely amorphous protein layer adsorption is not expected to show correlations in the encapsulation efficiency with size. However, size-dependent encapsulation can be an indicator of closed-shell formation (the occurrence of encapsulation is expected to decrease when the size of the gold particle exceeds the size of the cavity, for a given *T*-number). This is why studies of efficiency of encapsulation vs core size have been carried out.

*IV. In Vitro CLP Assembly with 48-mer Single-Stranded Nucleic Acid and Characterization.* In vitro CLP assembly was performed as described before[25,28] with slight modifications. Briefly, RRV CP was expressed in pET-29b (+) DNA plasmid (Novagen) in Rosetta2 cells until the $OD_{600}$ was 0.4−0.6. At that time, cells were induced with 1 mM ITPG and grown at 37 °C for 4 h before being harvested. Cells were lysed by French press, and the clarified lysate was applied to a High Trap SP FF 1 mL column. The protein was eluted with 500 mM NaCl in 20 mM Hepes and 2 mM EDTA, pH 8.0, concentrated, and buffer exchanged into HNE (20 mM HEPES:0.15 M NaCl:0.1 mM EDTA; pH 7.5). Protein concentrations were determined by the Bradford assay technique.

RRV CLPs with 48-mer DNA were formed under conditions described previously[25,28] in TNKM assembly buffer (50 mM Tris-HCl:50 mM NaCl:10 mM KCl:5 mM MgCl2; pH 7.4). This buffer was successfully used in the assembly of GNPs with brome mosaic virus (BMV) capsid proteins,[18,56] and it did not cause nanoparticle aggregation as seen with other assembly buffers. This change was not expected to affect the in vitro assembly of alphavirus CLP assembly since it was previously shown that a wide selection of assembly buffers is available for capsid formation.[25,28] The formation of CLPs was characterized by gel electrophoresis and TEM as described previously.[25] DLS and TEM measurements of RRV CLPs were compared with structural data of wt nucleocapsids.[28,30,31,33,40,41,57,58]

*V. Functionalized Au−CLP Assembly and Characterization Protocol.* For the self-assembly of CP around functionalized GNPs, we used 240 equiv of capsid protein monomers per functionalized GNP (corresponding to a T = 4 nucleocapsid) in TNKM buffer. GNP concentrations were determined by UV−vis spectroscopy, and protein concentrations were determined as mentioned above. Typical protein concentrations were 0.3−0.4 mg/mL and gold nanoparticle solutions were in the 100−800 nM range. Before assembly, the gold conjugate in 0.5× TBE buffer was sonicated for 30 min in cold water (8 °C). The required volume of CP in HNE buffer (described above) was then added to the nanoparticle solution. This step was immediately followed by the addition of the same volume of assembly buffer.

Reaction mixtures were incubated for 10 min at room temperature. Au−CLP solutions were stored at 4 °C. The formation of Au−CLPs was characterized by negative stain TEM and DLS. Prior to DLS measurements, all solutions were sonicated for 30 min to redisperse all possible large aggregates. TEM diameters were estimated using at least two grids, and DLS values were corroborated with three different preparations in each case.

**Results and Discussion.** *I. Influence of Electrostatics in Templating Au−CLP Formation.* As a control for our nanoparticle assembly protocol, we formed RRV CLPs with 48-mer DNA, as previously described.[25,28] The assembly

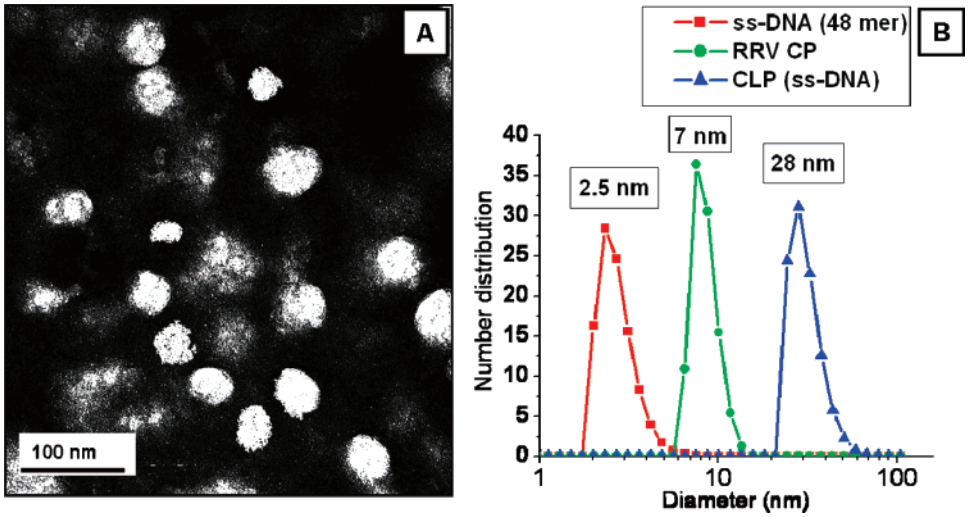


**Figure 2.** In vitro assembly of RRV CLPs. (A) Negatively stained TEM images of RRV CLPs measured 36.9 ± 5 nm. (B) Scattered light of the nucleocapsids (28 nm) reveals an increment in the hydrodynamic diameter compared to RRV CP and single strands of 48-mer DNA.

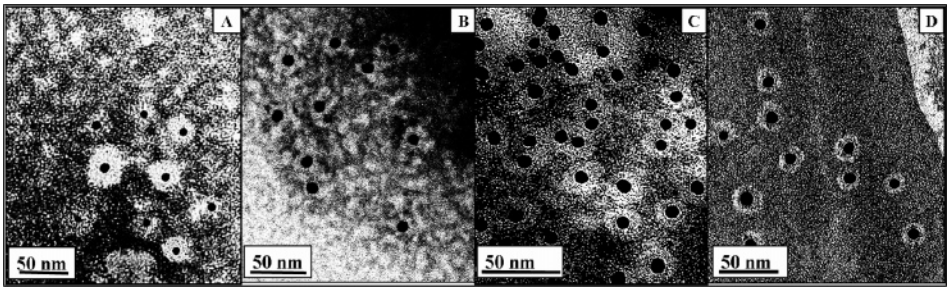


**Figure 3.** Negative staining TEM images of RRV CLPs: (A) 9 nm Au core diameter, P−Au−CLP diameter 32 ± 4 nm; (B) 10 nm Au core size, one 30-mer DNA/phosphane−Au−CLP diameter 29 ± 3.5 nm; (D) 11.5 nm Au core diameter; (C) 10 nm Au core size, 30-mer DNA/OMe−PEG−Au−CLP (diameter: 28.3 ± 7 nm); (D) 48-mer DNA/p−Au−CLP (diameter: 38 ± 3.7 nm).

reaction yielded particles of 36.9 ± 5 nm (~800 particles), as measured by TEM (Figure 2A), in agreement with the literature.[28,30,31,40,41,57,58] For clarity, it is important to note that the reported dimensions for the wt nucleocapsid core range from 38[34,57] to 40 nm[31,40,41] in diameter while the entire virion measured between 68[34,58] and 71 nm[31,41] in diameter.

The DLS data indicated an average hydrodynamic diameter of ~28 nm. The smaller sizes detected by DLS (Figure 2B) compared to TEM could be the result of averaging between intact CLPs, side products from the CP expression system, and protein intermediates unable to self-assemble into CLPs. It is interesting to note that viral particles that have been used in nanotechnology include CPMV, CCMV, CPV, and MS2, all of which have a diameter between 25 and 30 nm[3]. The significance, if any, of this size consistency is unknown.

To form RRV CLP encapsulating nanoparticles, we used negatively charged, 12 nm diameter, phosphane-coated GNPs (p−Au). The p−Au GNPs were mixed with 1 equiv of RRV CP to prepare p−Au−CLPs.

Negatively stained electron micrographs of p−Au and RRV CP clearly indicate that protein adsorption onto the nanoparticle surface process had occurred, Figure 3A. This is not surprising because RRV CP is basic, especially in the N-terminus region, with the entire protein having a pI > 9.5. The average diameter of the protein shell measured by TEM was 32 ± 4 nm (400 particles). The difference in thickness of the light shell seen around the GNPs before and after the encapsidation protocol indicates the deposition of the positively charged CP around the negatively charged p−Au. However, the average thickness of the CP shell (10 nm) in p−Au−CLPs was greater than the expected thickness of the wild type nucleocapsid (5 nm).[28,31] The thick protein packing in p−Au−CLP suggests either protein multilayers around gold or a denaturated protein layer, at least in the conditions required for TEM analysis.

TEM imaging of 48-mer CLP and p−Au−CLPs showed more irregular CLP formation compared to 48-mer CLPs (Figure 2A vs Figure 3A). This observation suggests possible denaturation caused by hydrophobic direct interactions of the CP with the metallic surface. In addition, DLS experiments on p−Au−CLPs resulted in an average particle diameter of 34 nm (Figure 4). In this case, DLS gave a large diameter particle than TEM, contrary to what was seen with other samples. Compared to the 28 nm diameter obtained for RRV CLPs, this result is consistent with p−Au−CLP having multiple protein layers or the DLS, reflecting the average of multiple species present in the heterogeneous mixture.

We deduce that, although p−Au−CLPs are unlikely to be similar to wt nucleocapsids, a first step of electrostatic recruitment of the protein by the anionic core does occur

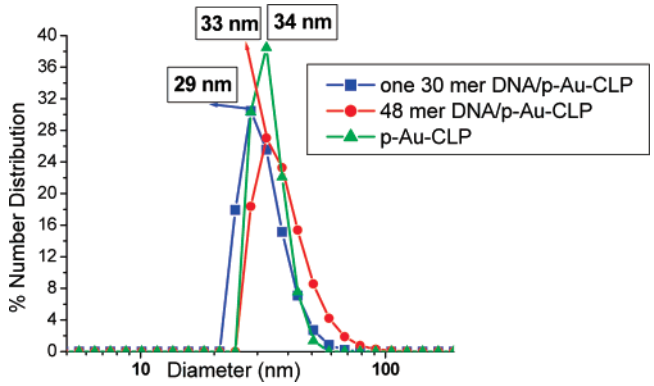


**Figure 4.** DLS size distribution of various functionalized GNPs (9−11.5 nm) after assembly with RRV CP. The hydrodynamic radius of one 30-mer DNA/p−Au−CLP, 48-mer DNA/p−Au−CLP, and p−Au−CLP is shown as a function of the Au surface coating after assembly; 30-mer DNA/p−Au−CLPs measured 29 nm by TEM and DLS, but 48-mer DNA/p−Au−CLPs measured 33 nm by DLS and 30 nm by TEM. p−Au−CLPs measured 32 nm by TEM and 34 nm by DLS.

and it results in complexes that have protein multilayers or a disorganized protein shell.

*II. Influence of Partial and Complete ssDNA Templating in Au−CLP Formation.* To test the hypothesis that CLP formation may be dependent on an initial binding and nucleation event between nucleic acid and capsid protein, a single 30-base ss-DNA modified with a thiol group at its 5′ end (HS-$(CH_2)_6OPO_3$-5′-GTCTTCCGCTCTCGGCAGAG-GTGTGAAGGA-3′)) was coupled to the p−Au particle. The new core is termed here 30-mer DNA/p−Au−CLP. The product of the CP association with p−Au conjugates containing only one ss-DNA was a one 30-mer DNA/p−Au−CLP of 29 ± 3.5 nm in average (as measured by TEM and confirmed by DLS) (Figure 3B).

TEM images (Figure 3B) of one 30-mer DNA/p−Au−CLPs reveal the formation of incomplete or deformed CLPs and/or inability of the CP associated with the core to rearrange into a closed shell. To determine if the CP shell symmetry will improve by coating the entire p−Au core with a uniform layer of 30-base ss-DNA instead of a single strand, we have coated the Au particles with a monolayer of 30-base ss-DNA and thiol methoxy PEG (1 Au:748 DNA:748 PEG). These cores are termed 30-mer DNA/OMe−PEG−Au.

Addition of CP to these conjugates resulted in 30-mer DNA/OMe−PEG−Au−CLPs (Figure 3C) measuring 28.3 ± 7 nm (by TEM, 400 particles counted). The white protein ring was around 6 nm thick. This is close to the expected wt protein shell thickness and suggests a single protein layer around the gold surface.

Visually, the 30-mer DNA/OMe−PEG−Au−CLPs were more spherical and the ensemble more homogeneous when compared to the case of one 30-mer DNA/p−Au−CLPs. However, the number of encapsulated particles seen on TEM (∼40 out of a total of 500 imaged particles) indicated a low efficiency of incorporation, which might suggest that a minimum surface charge density as well as DNA−CP interactions throughout the entire surface capsid/core interface are required for encapsulation. This minimum charge density requirement may not be met by 30-mer DNA/OMe−PEG−Au nanoparticles due to the fact that the thiolated methoxy PEG is not charged and it carries only the role of hydrophilic protectant of the Au surface.

Therefore, the unspecific DNA sequence (30-mer) has been replaced by an alphavirus specific DNA (48-mer) sequence and we used phosphane-coated GNPs instead of pegylated GNPs. Phosphane molecules are smaller than thiolated PEG molecules and therefore offer less steric hindrance when thiolated 48-mer DNA ligands are used for exchange. The anionic charge density is also expected to be higher.

*III. DNA-Saturated Nanoparticle Templates.* A nanoparticle template was constructed by coating GNPs with 48-base ss-DNAs modified with thiols at the 5′ end: (HS-$(CH_2)_6OPO_3$-5′-CCGTTAATGCATGTCGAGATATAAA-GCATAAGGGACATGCATTAACGG-3′), which resembles the alphavirus encapsidation signal from the genomic RNA.[46] This sequence is predicted to have a stem loop with CP affinity in its secondary structure.[46]

Addition of RRV CP to these conjugates in solution produced homogeneous 48-mer DNA/p−Au−CLPs (Figure 3D) measuring 38 ± 3.7 nm in diameter (∼800 particles counted), which is close to the CLP dimensions measured by TEM (Figure 2A). Negatively stained TEM images of 48-mer DNA/p−Au−CLPs show a clear 13 nm white ring assembled around the 48-mer DNA/p−Au, from which ∼5 nm corresponds to the naked 48-mer DNA/p−Au conjugates. A comparison between the size of these conjugates before and after the assembly protocol suggests that the space occupied by the CP is around 7 nm, which is similar to the wt.[28,30,31,33,40,41,57,58] In addition, the DLS measurement gave a diameter of 33 nm for the encapsidated particles compared to 38 ± 3.7 nm from TEM. Smaller hydrodynamic radii are accounted for by the presence of unreacted species. We deduce therefore that both electrostatics and the presence of the encapsidation signal are sufficient for the efficient templated assembly of the Au−CLP.

*IV. CLP Stability as a Result of Purification of 48-mer DNA/p−Au.* Because the possible persistence of a loosely bound species of DNA at equilibrium with free DNA in solution remaining from the synthesis of 48-mer DNA/p−Au may be a part of the reassembly process, a multistep

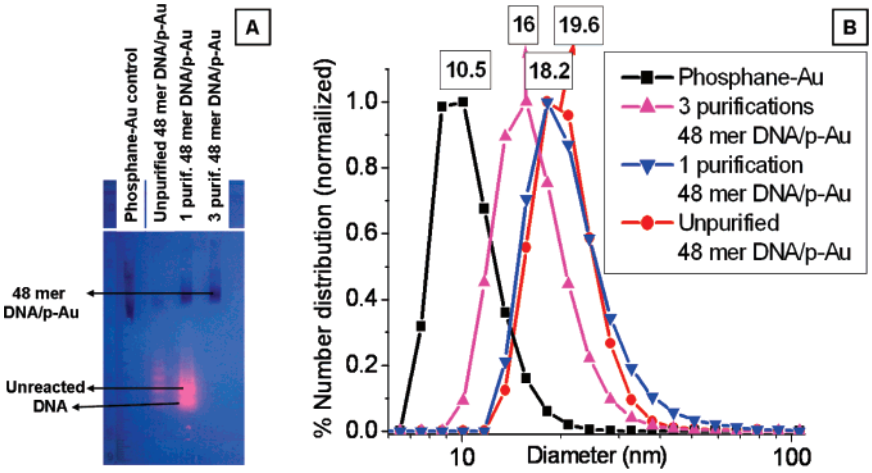


**Figure 5.** Effect on mobility and size when elimination of unbound DNA from 48-mer DNA/p−Au solution was performed. (A) Gel electrophoresis showed no free DNA present after three purifications. (B) After three purifications, the average diameter decreased ~4 nm.

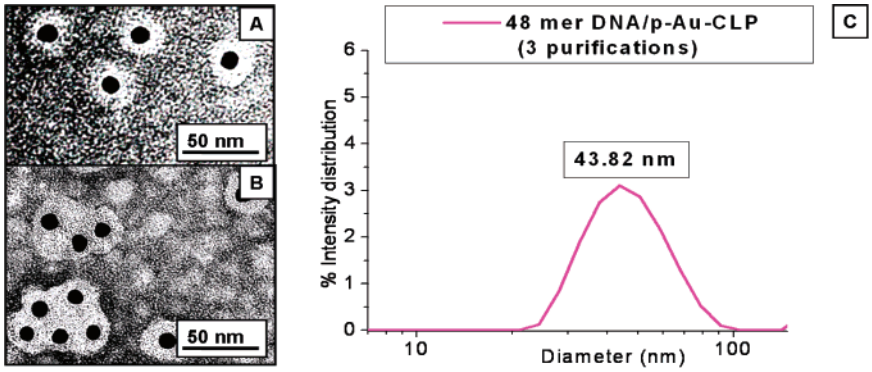


**Figure 6.** Au−CLP in vitro assembly under covalently bound DNA conditions. Three times purified 11.5 nm gold templates covered with DNA were mixed with stoichiometric amounts of RRV CP to produce Au−CLP, as illustrated in (A). The average diameter of these Au−CLPs was 31.6 ± 4 nm. Assembly with covalently bound DNA on the gold surface was only partially successful. Visible aggregation occurred within 1 h after assembly (B). The DLS of the Au−CLPs showed a broad peak with a mean at 43.82 nm (C).

purification was carried out in order to remove this excess DNA, Figure 5. After three purifications using size exclusion chromatography, all unbound DNA was removed, Figure 5. The outcome of the assembly reaction using 3× purified cores was analyzed by TEM and DLS (Figure 6).

Somewhat surprisingly, the 48-mer DNA/p−Au−CLPs assembled with the 3× purified conjugates were not as stable as the unpurified products. Negative staining TEM imaging of the 3× purified solution of 48-mer DNA/p−Au suggested that the purified particles are weak promoters of capsid assembly (Figure 6).

The purified 48-mer DNA/p−Au−CLPs visualized on TEM immediately after synthesis (Figure 6A) conserved spherical symmetry and size with respect to the unpurified 48-mer CLPs. The size distribution of these conjugates had a mean at 32 nm, which is close to the expected 37 nm for the wt. However, in time, a color change of the solution from red to blue was observed, indicating aggregation (Figure 6B,C). However, DLS taken 1 h after assembly (the shortest time possible between an assembly reaction and the DLS experiment) showed an evolving broad peak (Figure 6C), indicating that aggregation was still be taking place at the time of measurement.

Lower efficiencies of encapsulation and stability of Au−CLPs obtained from 3× purified 48-mer DNA/p−Au (Figure 6B) as compared with Au−CLPs, formed when free or loosely bound DNA is available (Figure 3D), seem to suggest that free-DNA may be required for better encapsulation.

A possible explanation could be that the amount of DNA present on the gold surface was not sufficient to prevent detrimental phosphane−CP interactions, which may be responsible for denaturation of the protein coat. When free DNA is present, DLS data indicates that some of it binds to the GNPs in addition to covalently bound DNA, thus decreasing the occurrence of direct phopshane−capsid interactions (Figure 5B).

Another explanation for the smaller number of Au−CLPs formed from purified nanoparticle reactant may be the requirement for a nucleoprotein early intermediate for CLP assembly, possible only when free oligo-DNA is present in the solution. However, to test this hypothesis, further studies are necessary.

DLS was used to compare the stability of the 48-mer DNA/p−Au−CLPs to a native CLP control, Figure 7. The hydrodynamic radii of the 48-mer DNA/p−Au−CLPs re-

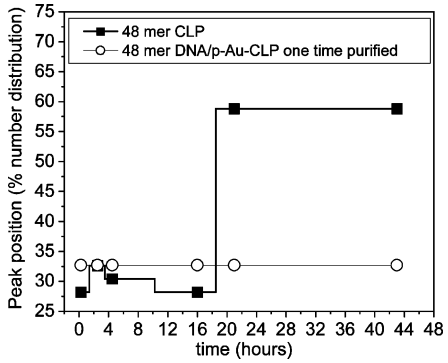


**Figure 7.** Stability of Au−CLPs and 48-mer CLPs as a function of time, as indicated by changes in the position of the peak of size distribution. The DLS of 1× purified 48-mer DNA/p−Au and 48-mer DNA with RRV CP were measured over a period of 10 min to 44 h after assembly at 8 °C.

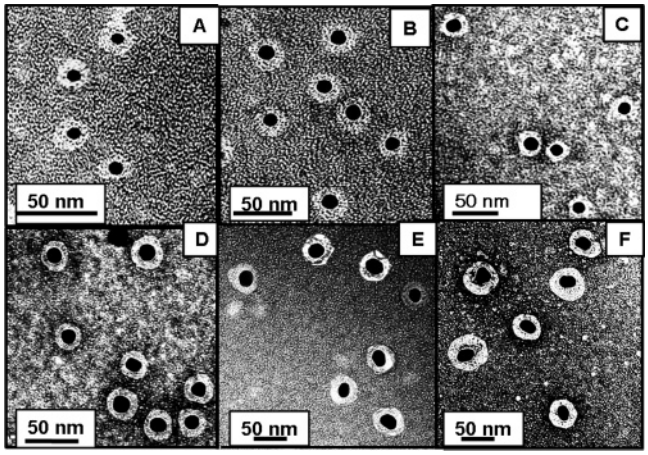


**Figure 8.** TEM images of encapsidated 48-mer DNA/p−Au particles with different sized Au cores: (A) 8.3 nm core size; (B) 11.5 nm core size; (C) 13.9 nm core size; (D) 18.7 nm core size; (E) 23.6 nm core size; (F) 27.4 nm core size. The equivalent ratios of Au (100−800 nM) to CP (0.3 mg/mL) are 1:240 for all the assemblies.

mained the same throughout the entire duration of experiment (44 h), while fluctuations and drift toward larger average diameters (aggregation) have been measured for the CLP control. Therefore, nanoparticle-encapsulating CLPs are more stable upon storage than their native counterparts.

*V. Influence of the Gold Core Size in Promoting DNA/p−Au−CLP Assembly.* Once the 1× purified 48-mer DNA/p−Au ligand was identified as most likely to yield efficient templated capsid growth, different GNP sizes were tested with respect to their encapsulation efficiency.

Six different sizes of functionalized GNPs were prepared using gold cores of 8.3, 11.5, 13.9, 18.7, 23.6, and 27.4 nm. DNA/p−Au conjugates were purified only once for the excess of nucleotide in solution. DNA/p−Au conjugates were then mixed with RRV CP in an assembly buffer. The assembly reaction led to the formation of 48-mer DNA/p−Au−CLPs accompanied, as expected, by an increment in the average particle diameter (Figure 8).

Negatively stained TEM images of encapsulated 48-mer DNA/p−Au of different sizes show the formation of spherical and homogeneous capsids, Figure 8. The DNA/p−Au−CLP complexes closest in size to the 48-mer CLP are obtained for 18.7 nm cores.

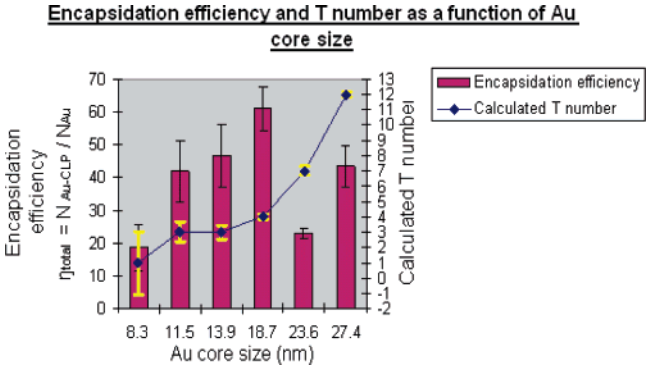


**Figure 9.** 48-mer DNA/p−Au nanoparticle encapsidation efficiencies as a function of GNP core size (vertical bars). Error bars represent standard deviations obtained from ensembles of ∼800 particles. Dependence of the *T* number on the core diameter estimated from the same particle populations.

Encapsulation efficiency for each nanoparticle diameter was estimated from TEM images and represented as a function of core size in Figure 9One notes on Figure 9 that, while the size of the CLP complex varied monotonically with the template diameter, the encapsidation efficiency reaches a maximum (62% at 18.7 nm) and then decreases significantly for larger nanoparticle diameters. A similar behavior has been observed for GNP encapsulation in BMV, pointing to a correlation between the *T*-number and the self-assembly efficiency.[16] Because of this correlation, it is possible that closed-shell formation occurs at least for certain core sizes. Among them, the 18.7 nm gold cores provide the highest average encapsulation yield (62%).

In addition to estimating efficiencies, the DNA/p−Au−CLP size distribution from TEM was used to compute possible triangulation numbers, *T*, for CLP polymorphs induced by the different core sizes. The equation proposed by Caspar and Klug[59] relates *T* with the diameter (*D*) of the icosahedral particle and *d*, when the center-to-center distance of the basic structural unit (capsomers)is known:[60]

$$T^{1/2} = \frac{0.618 \times D}{d}$$

The alphavirus nucleocapsid diameter measured from structural data has been found to be between 38 and 40 nm,[28,30,31,33,40,41,57,58] while the distance *d* between the capsomers (pentamers of CP) has been calculated to be between 12.04 nm and asuming a pseudo-$T = 4$ icosahedron.[60] The calculated triangulation numbers are plotted in Figure 10 against the core size and 48-mer DNA/p−Au encapsulation efficiencies. There is a plateau observed at $T = 4$, which also suggests a trend toward a predetermined arrangement of the CP into $T = 4$ icosahedron.[30,33,61] These observations are consistent with 48-mer CLPs and wt nucleocapsids, forming mostly $T = 4$ sized particles.

The *T* number corresponding to 18.7 nm GNPs is also associated with the wt CLP, found from structural data. In

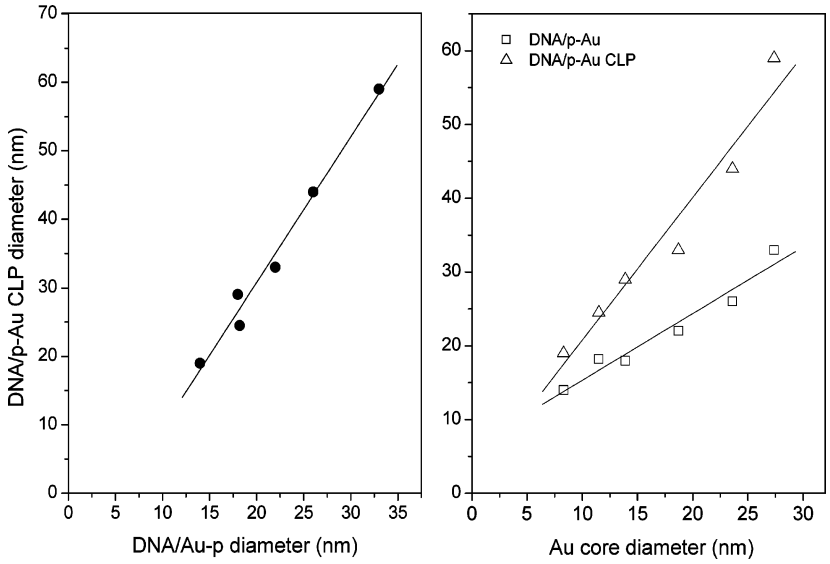


**Figure 10.** Plots of the CLP diameter vs the ligand-coated core diameter (left) and of the CLP and ligand-coated core diameter vs bare GNP diameter (right).

contrast, for bigger nanoparticle cores (23 and 27.4 nm), the Au−CLP T number seemed to increase linearly with the gold size, resulting in a possible $T = 7$ and $T = 12$, respectively. However, the linear increase may also indicate that CP failed to arrange into a regular quasispherical array.

A comparison between the DLS diameters of the DNA/p−Au particles before and after assembly with the RRV CP shows a linear increment with the size of the nanoparticle, Figure 10. In the case when a layer of protein of constant thickness is added, the slope of the CLP diameter vs DNA/Au−p diameter is expected to be 1 because:

$$D_{\mathrm{CLP}} = D_{\mathrm{GNP}} + 2 \times t$$

where: $D_{\mathrm{CLP}}$ = CLP diameter, $D_{\mathrm{GNP}}$ = diameter of the nanoparticle core (DNA/Au−p), and $t$ = thickness of the molecular (ligand + protein) layer.

In Figure 10, the slope is 2.0 ± 0.1, which implies that the thickness of the protein plus ligand layer depends linearly on the radius of the core, at least for the size range of 7−30 nm. The question is, does the ligand layer or the protein layer thickness vary with the size of the nanoparticle template? To answer this question, Figure 10 (right) shows how the ligand layer and the protein + ligand layer thicknesses vary with the nanoparticle template diameter. Again, we observe a linear dependence in both cases. However, the linear fit corresponding to the ligand layer has a slope of 1, which implies a constant ligand thickness (of ∼3 nm), independent of Au core size. Therefore, it is the thickness of the protein shell that varies with the radius of the spherical template. Larger cores seem to induce a thicker protein shell, which raises the question of the nature of the shell. However, structural studies are necessary in order to answer this question. This report provides ways to obtain a large amount of homogeneous sample, therefore opening the door for structural studies and progress toward a complete alphavirus nanoparticle carrier.

**Conclusion.** We have shown that functionalized GNPs can be used as templates to promote the self-assembly of an animal virus capsid protein shell. A maximum encapsidation yield of 62% has been obtained for core nanoparticles having a diameter of 18.7 nm. The products of nanoparticle-templated growth tend to be more stable upon storage than empty CLPs. Similar to the case of the brome mosaic plant virus, maximum efficiency correlates with capsid-like particle increased stability and diameters that are close to the wt CLP diameter. Charge neutralization is necessary but not sufficient to drive Au−CLP assembly, unlike the case of previously studied nonenveloped plant viruses. The main specific difference for alphavirus CLPs is the requirement for the existence of encapsidation signal DNA free in solution simultaneously with adsorbed DNA on the artificial cores.

**Acknowledgment.** We gratefully acknowledge NSF support (CBET award nos. 0730149 and 0631982).

## References

(1) Torchilin, V. P. *Adv. Drug Deliv. Rev.* **2006**, *58*, 1532−1555.
(2) Lundstrom, K. *Gene Ther.* **2005**, *12*, S92−S97.
(3) Manchester, M.; Singh, P. *Adv. Drug Delivery Rev.* **2006**, *58*, 1505−1522.
(4) Lewis, J. D.; Destito, G.; Zijlstra, A.; Gonzalez, M. J.; Quigley, J. P.; Manchester, M.; Stuhlmann, H. *Nat. Med.* **2006**, *12*, 354−360.
(5) Anderson, E. A.; Isaacman, S.; Peabody, D. S.; Wang, E. Y.; Canary, J. W.; Kirshenbaum, K. *Nano Lett.* **2006**, *6*, 1160−1164.
(6) Douglas, T.; Young, M. *Science* **2006**, *312*, 873−875.
(7) Nam, K. T.; Kim, D. W.; Yoo, P. J.; Chiang, C. Y.; Meethong, N.; Hammond, P. T.; Chiang, Y. M.; Belcher, A. M. *Science* **2006**, *312*, 885−888.
(8) Singh, P.; Gonzalez, M. J.; Manchester, M. *Drug Dev. Res.* **2006**, *67*, 23−41.
(9) Katz, E.; Shipway, A. N.; Willner, I. Biomaterial−Nanoparticle Hybrid Systems: Synthesis, Properties, and Applications. In *Nanoparticles*; Schmid, G., Ed.; Wiley-VCH: Weinheim, 2004.
(10) Lin, A. W. H.; Lewinski, N. A.; West, J. L.; Halas, N. J.; Drezek, R. A. *J. Biomed. Opt.* **2005**, *10*, 064035.
(11) Raja, K. S.; Wang, Q.; Gonzalez, M. J.; Manchester, M.; Johnson, J. E.; Finn, M. G. *Biomacromolecules* **2003**, *4*, 472−476.
(12) Ochoa, W. F.; Chatterji, A.; Lin, T.; Johnson, J. E. *Chem. Biol.* **2006**, *13*, 771−778.

(13) Tseng, J. C.; Levin, B.; Hurtado, A.; Yee, H.; de Castro, I. P.; Jimenez, M.; Shamamian, P.; Jin, R. Z.; Novick, R. P.; Pellicer, A.; Meruelo, D. *Nat. Biotechnol.* **2004**, *22*, 70−77.
(14) Yacoby, I.; Shamis, M.; Bar, H.; Shabat, D.; Benhar, I. *Antimicrob. Agents Chemother.* **2006**, *50*, 2087−2097.
(15) Hooker, J. M.; Kovacs, E. W.; Francis, M. B. *J. Am. Chem. Soc.* **2004**, *126*, 3718−3719.
(16) Sun, J.; DuFort, C.; Daniel, M.-C.; Murali, A.; Chen, C.; Gopinath, K.; Stein, B.; De, M.; Rotello, V. M.; Holzenburg, A.; Kao, C. C.; Dragnea, B. *Proc. Natl. Acad. Sci. U.S.A.* **2007**, *104*, 1354−1359.
(17) Dragnea, B.; Chen, C.; Kwak, E. S.; Stein, B.; Kao, C. C. *J. Am. Chem. Soc.* **2003**, *125*, 6374−6375.
(18) Chen, C.; Daniel, M. C.; Quinkert, Z. T.; De, M.; Stein, B.; Bowman, V. D.; Chipman, P. R.; Rotello, V. M.; Kao, C. C.; Dragnea, B. *Nano Lett.* **2006**, *6*, 611−615.
(19) Loo, L.; Guenther, R. H.; Basnayake, V. R.; Lommel, S. A.; Franzen, S. *J. Am. Chem. Soc.* **2006**, *128*, 4502−4503.
(20) Griffin, D. E. *Semin. Virol.* **1995**, *6*, 249−255.
(21) Pasquato, L.; Pengo, P.; Scrimin, P. Biological and Biomimetic Applications of Nanoparticles. In *Nanoparticles, Building Blocks for Nanotechnology*; Rotello, V. M., Ed.; Springer: Amherst, MA, 2004.
(22) Kumar, M. N. V. R.; Bakowsky, U.; Lehr, C.-M. Nanoparticles as Non-Viral Transfection Agents. In *Nanobiotechnology*; Niemeyer, C., Mirkin, C., Eds.; Wiley-VCH: Weinheim, 2004.
(23) Klimstra, W. B.; Williams, J. C.; Ryman, K. D.; Heidner, H. W. *Virology* **2005**, *338*, 9−21.
(24) Strauss, J. H.; Strauss, E. G. *Microbiol. Rev.* **1994**, *58*, 491−562.
(25) Tellinghuisen, T. L.; Hamburger, A. E.; Fisher, B. R.; Ostendorp, R.; Kuhn, R. J. *J. Virol.* **1999**, *73*, 5309−5319.
(26) Tellinghuisen, T. L.; Perera, R.; Kuhn, R. J. *J. Virol.* **2001**, *75*, 2810−2817.
(27) Perera, R.; Owen, K. E.; Tellinghuisen, T. L.; Gorbalenya, A. E.; Kuhn, R. J. *J. Virol.* **2001**, *75*, 1−10.
(28) Mukhopadhyay, S.; Chipman, P. R.; Hong, E. M.; Kuhn, R. J.; Rossmann, M. G. *J. Virol.* **2002**, *76*, 11128−11132.
(29) Marsh, M.; Helenius, A. *Cell* **2006**, *124*, 729−740.
(30) Mukhopadhyay, S.; Zhang, W.; Gabler, S.; Chipman, P. R.; Strauss, E. G.; Strauss, J. H.; Baker, T. S.; Kuhn, R. J.; Rossmann, M. G. *Structure* **2006**, *14*, 63−73.
(31) Zhang, W.; Mukhopadhyay, S.; Pletnev, S. V.; Baker, T. S.; Kuhn, R. J.; Rossmann, M. G. *J. Virol.* **2002**, *76*, 11645−11658.
(32) Pletnev, S. V.; Zhang, W.; Mukhopadhyay, S.; Fisher, B. R.; Hernandez, R.; Brown, D. T.; Rossmann, M. G.; Kuhn, R. J. *Cell* **2001**, *105*, 127−136.
(33) Mancini, E. J.; Clarke, M.; Gowen, B. E.; Rutten, T.; Fuller, S. D. *Mol. Cell* **2000**, *5*, 255−266.
(34) Paredes, A.; Alwell-Warda, K.; Weaver, S. C.; Chiu, W.; Watowich, S. J. *J. Virol.* **2001**, *75*, 9532−9537.
(35) Strauss, J. H.; Strauss, E. G. *Microbiol. Rev.* **1994**, *58*, 491−562.
(36) Datwyler, D. A.; Eppenberger, H. M.; Koller, D.; Bailey, J. E.; Magyar, J. P. *J. Mol. Med.* **1999**, *77*, 859−864.
(37) Frolov, I.; Hoffman, T. A.; Pragai, B. M.; Dryga, S. A.; Huang, H. V. *Proc. Natl. Acad. Sci. U.S.A.* **1996**, *93*, 11371−11377.
(38) Nargi-Aizenman, J. L.; Griffin, D. E. *J. Virol.* **2001**, *75*, 7114−7121.
(39) Perri, S.; Greer, C. E.; Thudium, K.; Doe, B.; Legg, H.; Liu, H.; Romero, R. E.; Tang, Z. Q.; Bin, Q.; Dubensky, T. W.; Vajdy, M.; Otten, G. R.; Polo, J. M. *J. Virol.* **2003**, *77*, 10394−10403.
(40) Zhang, W.; Fisher, B. R.; Olson, N. H.; Strauss, J. H.; Kuhn, R. J.; Baker, T. S. *J. Virol.* **2002**, *76*, 7239−7246.
(41) Zhang, W.; Heil, M.; Kuhn, R. J.; Baker, T. S. *Virology* **2005**, *332*, 511−518.
(42) Hong, E. M.; Perera, R.; Kuhn, R. J. *J. Virol.* **2006**, *80*, 8848−8855.
(43) Perera, R.; Navarantnarajah, C.; Kuhn, R. J. A *J. Virol.* **2003**, *77*, 8345−8353.
(44) Schneemann, A.; Gallagher, T. M.; Rueckert, R. R. *J. Virol.* **1994**, *68*, 4547−4556.
(45) Ceres, P.; Stray, S. J.; Zlotnick, A. *J. Virol.* **2004**, *78*, 9538−9543.
(46) Wengler, G.; Wengler, G.; Boege, U.; Wahn, K. *Virology* **1984**, *132*, 401−412.
(47) Bradley, J. S.; Schmid, G. Noble Metal Nanoparticles. In *Nanoparticles*; Schmid, G., Ed.; Wiley-VCH: Weinheim, 2004.
(48) Forsell, K.; Griffiths, G.; Garoff, H. *EMBO J.* **1996**, *15*, 6495−6505.
(49) Slot, J. W.; Geuze, H. J. *Eur. J. Cell Biol.* **1985**, *38*, 87−93.
(50) Frens, G. *Nat. Phys. Sci.* **1973**, *241*, 20−22.
(51) Zhu, T.; Vasilev, K.; Kreiter, M.; Mittler, S.; Knoll, W. *Langmuir* **2003**, *19*, 9518−9525.
(52) Loweth, C. J.; Caldwell, W. B.; Peng, X.; Alivisatos, A. P.; Schultz, P. G. *Angew. Chem., Int. Ed.* **1999**, *38*, 1808−1812.
(53) Zanchet, D.; Micheel, C. M.; Parak, W. J.; Gerion, D.; Alivisatos, A. P. *Nano Lett.* **2001**, *1*, 32−35.
(54) Parak, W. J.; Pellegrino, T.; Micheel, C. M.; Gerion, D.; Williams, S. C.; Alivisatos, A. P. *Nano Lett.* **2003**, *3*, 33−36.
(55) Kimura, K.; Takashima, S.; Ohshima, H. *J. Phys. Chem. B* **2002**, *106*, 7260−7266.
(56) Chen, C.; Kwak, E. S.; Stein, B.; Kao, C. C.; Dragnea, B. *J. Nanosci. Nanotechnol.* **2005**, *5*, 2029−2033.
(57) Paredes, A.; Alwell-Warda, K.; Weaver, S. C.; Chiu, W.; Watowich, S. J. *J. Virol.* **2003**, *77*, 659−664.
(58) Paredes, A.; Weaver, S.; Watowich, S.; Chiu, W. *Arch. Virol.* **2005**, 179−185.
(59) Caspar, D. L. D.; Klug, A. *Cold Spring Harbor Symp. Quantum Biol.* **1962**, *27*, 1−24.
(60) Ferreira, D.; Hernandez, R.; Horton, M.; Brown, D. T. *Virology* **2003**, *307*, 54−66.
(61) Mukherjee, S.; Pfeifer, C. M.; Johnson, J. M.; Liu, J.; Zlotnick, A. *J. Am. Chem. Soc.* **2006**, *128*, 2538−2539.

NL070860E